The Astronomical Journal, 161:259 (5pp), 2021 June https://doi.org/10.3847/1538-3881/abf55d

Time-domain Modulation of HD 189733 Activities by Its Planet

Yang Gao[1,2]
[1] School of Physics and Astronomy, Sun Yat-Sen University, Zhuhai 519082, Guangdong, People's Republic of China
[2] CAS Key Laboratory of FAST, National Astronomical Observatories, Chinese Academy of Sciences, Beijing 100101, People's Republic of China
Received 2020 September 9; revised 2021 April 5; accepted 2021 April 5; published 2021 May 7

Abstract

Star–planet interaction can be studied by analyzing exoplanetary orbit and stellar rotation modulations of the transit emissions from exoplanetary systems. Here we carry out a time-domain analysis of the multiband activities of the HD 189733 star–planet system observed in X-ray, atomic lines, and broadband spectra reported in the literature. We find that the number of activities occuring at beat angles (of the planetary orbit and the stellar rotation) concentrating on a sector with a width of 108° are significantly larger than expected from a uniform distribution of activities, which indicates the existence of a major stellar active magnetic field region. The concentration of activities in this active magnetic field region shows their possible origins from the magnetic field interaction between HD 189733 and its close planet HD 189733 b.

Unified Astronomy Thesaurus concepts: Exoplanets (498); Stellar flares (1603)

1. Introduction

Star–planet interaction (SPI) reveals the magnetic field environment of an exoplanet and its host star, and has been explored through X-ray, radio, and optical/FUV atomic lines toward a few systems (Shkolnik et al. 2003, 2005, 2008; Smith et al. 2009; Maggio et al. 2015; Pillitteri et al. 2015; Bower et al. 2016; Cauley et al. 2019; Route 2019). For a planet enclosed in the magnetosphere of its host star, SPI is expected to correlate with the beat period of the planetary orbit and stellar rotation as a result of the nonaxisymmetry of the stellar magnetic field (Fares et al. 2010). With similar magnetic field structures between the host and its companion, the time-domain features of the nonthermal emission from a host star induced by the hot Jupiter enclosed in its magnetosphere is expected to be similar to the emission from Jupiter induced by its satellite, Ganymede, with both sources originating from the magnetic reconnection (MRX) of the interacting magnetic fields of the host and its companion (Zarka 2007, 2018). In the Jovian system, radio flare rates have been found to be definitely correlated with both the Jovian rotation and the Ganymede orbit. The emissions induced by Jovian satellite Ganymede are observed at two distinct observer's Jovian central meridian longitudes (CML), and distribute at one sector covering ∼150° of the satellite's Jovicentric longitude (Zarka et al. 2018). However, different from the observation of the Jovian system, flares from stars with exoplanets are much less detected, thus it is impossible to use the 2D host rotation and companion orbit phase diagram, as in Zarka et al. (2018), to find the flare time-domain features. Instead, here we check the 1D correlations of the system activities to the beat phase of the stellar rotation and the exoplanetary orbit, as well as the stellar rotation period itself separately.

Among the exoplanetary systems with activities detected, HD 189733 has the most extensive observations. It is a K2V type star 19.3 pc from the Sun, and hosts a transit hot Jupiter HD 189733 b with an orbital distance 0.031 au, which is about nine times the stellar radius (Bouchy et al. 2005; Fares et al. 2017). As planet HD 189733 b is very likely enclosed in the stellar magnetosphere, SPI in this system is expected and has been explored through multiband observations (Shkolnik et al. 2008; Smith et al. 2009; Lecavelier des Etangs et al. 2009, 2012; Fares et al. 2010, 2017; Cauley et al. 2015, 2017; Route 2019; Bourrier et al. 2020). Although no radio detection has been made, observations of X-ray flares from HD 189733 confirm the existence of synchrotron emissions (Pillitteri et al. 2010, 2011, 2014; Poppenhaeger et al. 2013). The optical/FUV atomic line and broadband spectra observations, which are more commonly used to study the stellar atmosphere, magnetic field, and starspot activities, can also be informative of the magnetic field SPI (Pont et al. 2007; Sing et al. 2011; Czesla et al. 2015; Pillitteri et al. 2015). We thus combine all these observed activities and make further selections for a statistical analysis in this paper.

2. SPI Activities Induced by MRX

The most recent Juno observations indicate that the plasma sheet boundary layer of the Jovian magnetosphere originates from the Jovian rotation-dominated MRX (Zhang et al. 2000). Considering the favorable reconnection condition at the interaction site of Ganymede's and Jovian magnet fields, MRX that occurs at the upstream magnetopause of Ganymede is a significant source of the energetic particles; additionally, this Ganymede-related MRX has a reconnection rate that correlates with its orbital position (Kaweeyanun et al. 2020). The energetic particles produced in the Jupiter–Ganymede MRX have been estimated to be $E_{\rm J-G} = 2.9$–48 keV (Ip & Kopp 2002); considering the magnetic field of $B_{\rm J-G} = 0.02$ G, this particle energy consistently leads to the nonthermal radiation frequency of a couple dozen megahertz observed in radio flares (Zarka et al. 2018). Scaling up the particle energy from the Jupiter–Ganymede MRX site with a magnetic field, $B_{\rm J-G}$, to that in the magnetized star–hot Jupiter systems with a local magnetic field of $B_{\rm s-hJ} \sim 2$ G, energetic particles of $E_{\rm s-hJ} = E_{\rm J-G} \cdot \frac{B^2_{\rm s-hJ}}{B^2_{\rm J-G}} \sim 10$–$100$ MeV are expected in the star–hot Jupiter systems. Such energetic electrons will lead to synchrotron flares at frequencies around a few gigahertz with fluxes that can be observable using state-of-the-art radio telescopes (Zarka et al. 2019; Gao et al. 2020).

For star–planet systems with magnetic field connections, the interaction between the stellar magnetosphere and the planetary magnetic field also induces MRX, which has already been considered a reasonable energy source of the X-ray flares (Maggio et al. 2015; Lanza 2018). Relativistic electrons produced in the

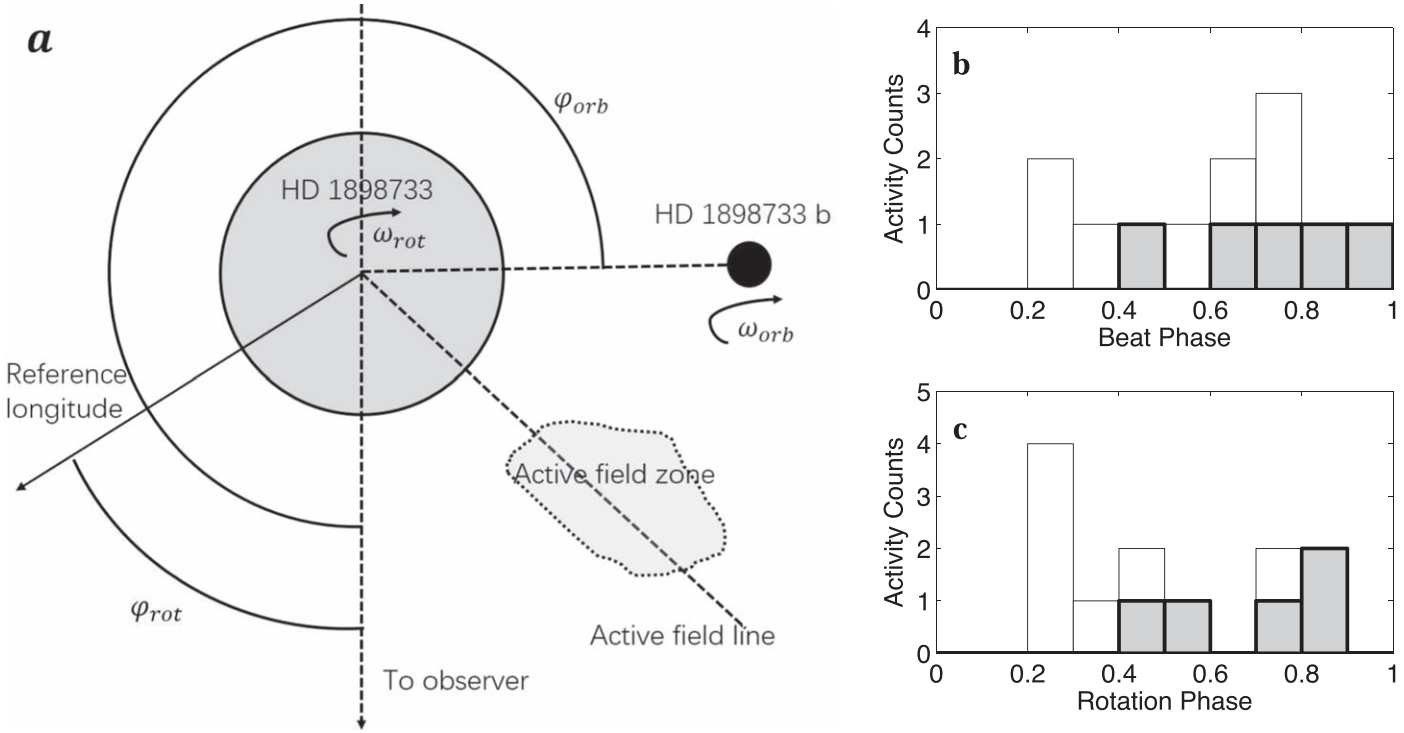

Figure 1. Star–planet magnetic field interaction and the activity phase distribution in HD 189733. Panel a illustrates the magnetic field SPI in HD 189733 system. The planet orbits the star at an angular speed of $\omega_{\rm orb}$; the schematic active magnetic field line has a fixed stellar longitude and corotates with the star at $\omega_{\rm rot}$. SPI occurs when the planet encounters the active field region. Panels b and c show the distributions of the HD 189733 activities in the beat phase and stellar rotation phase, respectively. Activities observed in all wave bands are included, with X-ray flares in gray bars. A concentration of activities in beat phases 0.6–0.9 can be identified and concentrations in stellar rotation phases 0.2–0.5 and 0.7–0.9 are noted.

MRX give rise to synchrotron emissions in both radio and X-ray bands when they travel along the star–planet magnetic field (Wang & Loeb 2019). Considering the nonaxisymmetry of the stellar magnetic field, MRX is more violent and frequent when the planet encounters the stronger and more active regions of the stellar magnetosphere, leading to more observable synchrotron flares. For atomic lines and broadband spectra, variation of the emission strength is also expected when the planet passes through the active regions of the stellar magnetic field (Fares et al. 2010, 2017; Donati et al. 2016, 2017; Cauley et al. 2019). So the rate of observed multiband activity is expected to be higher in the stellar active magnetic field region, i.e., modulated by the beat period of the planetary orbit and stellar rotation. Additionally, because of the beaming effect of synchrotron emission and the geometry of magnetic field lines, such activities are more observable when the observer's stellar CML is at one or two specified angles.

Following the illustration of Jupiter–satellite interactions (Zarka 2018), we schematically demonstrate the stellar rotation phase $\varphi_{\rm rot}$ and exoplanetary orbit phase $\varphi_{\rm orb}$ in Figure 1(a). The active field line, which has a fixed stellar longitude and corotates with the star at an angular speed of $\omega_{\rm rot}$ is also shown; the planetary orbit angular speed is $\omega_{\rm orb}$, and the beat angular speed is $\omega_{\rm beat} = \omega_{\rm orb} - \omega_{\rm rot}$. It is noted that the differential rotation of HD 189733 leads to a variable magnetic field during 2007 and 2015 (Fares et al. 2017), but there exists a major strong magnetic field region at longitudes around $\sim$100°–150° throughout. So for the SPI activities induced by MRX, a concentration of their beat phases when planet HD 189733 b passes this region is expected.

3. Magnetic SPI in the HD 189733 System

3.1. Candidate MRX Activities

Activities related to MRX behave as bursts at corresponding wavelength or emission/absorption lines. So we chose bursty activities whose fluxes are significantly higher than the out-of-burst emissions. Route (2019) reviewed the multiband observations of HD 189733 activities in the literature and summarized them in their Table 2. We first delete the nondetections in this data set, and add a new event from Bourrier et al. (2020) to construct our database shown in the first half of Table 1. Additionally, existing periodic variations following the planetary orbit are not included, such as most of the Ca II H and K observations (Shkolnik et al. 2008; Fares et al. 2017; Cauley et al. 2019). Differently, the Ca II H and K observations from Czesla et al. (2015) show an abrupt increase of flux (their Figure 11), which may result from the increase of the magnetic field activity level, so we keep it in Table 1. For the other two commonly observed atomic lines, the change in the Hα line strength is possibly caused by the circumplanetary absorptions, thus more often observed at pre- and post-transits of planets (Cauley et al. 2017), or sometimes irrelevant of the planet (Barnes et al. 2016; Guilluy et al. 2020). A Lyα variation is believed to have origins from the planetary upper atmosphere (Bourrier et al. 2020). So activities observed in Hα, or in only the Lyα lines, are removed from our database. Broadband continuum emissions, although they have been explained by the existence of starspots (Pont et al. 2007; Sing et al. 2011), can also be signatures of magnetic field activities, so we keep them in Table 1. However, one of the continuum emission activities (the green curve of Figure 1 in Pont et al. 2007) cannot be well

Table 1
HD 189733 Observed Activities and X-Ray Observations without Detection of Flares

ID	JD 2450000+	Orbital Phase	Rotation Phase	Beat Phase	Duration of Burst (ks)	Observation Band	Reference
01	3882.327	0.01	0.26	0.75	1.9	Broadband	Pont+ 07
02	3931.145	0.01	0.36	0.65	>0.3	Broadband	Pont+ 07
03	4970.624	0.54	0.71	0.84	7.0	X-ray	Pillitteri+ 10
04	5155.764	0.99	0.27	0.73	1.3	Broadband	Sing+ 11
05	5682.721	0.51	0.55	0.96	(1.2)	X-ray	Pillitteri+ 11
06	5812.125	0.84	0.42	0.42	(<1.0)	X-ray	Lecavelier des Etangs+ 12
07	6055.563	0.56	0.88	0.69	4.5	X-ray	Pillitteri+ 14
08	6055.736	0.64	0.89	0.75	10.0	X-ray	Pillitteri+ 14
09	6109.764	0.99	0.43	0.56	7.7	Ca II, H, K	Czesla+ 15
10	6422.554	0.98	0.71	0.26	(1.0)	Si III, Lyα	Bourrier+ 20
11	6547.981	0.51	0.26	0.26	(0.6)	Si III, C II, N V	Pillitteri+ 15
12	6548.123	0.58	0.27	0.31	(0.6)	Si III, C II, N V	Pillitteri+ 15
N1	4208.43	0.00	0.66	0.34	55.0	X-ray No-flare	Pillitteri+ 10
N2	5748.11	0.98	0.04	0.94	19.2	X-ray No-flare	Poppenhaeger+ 13
N3	5754,76	0.98	0.60	0.38	19.8	X-ray No-flare	Poppenhaeger+ 13
N4	5759.18	0.97	0.97	0.00	19.8	X-ray No-flare	Poppenhaeger+ 13
N5	5761.41	0.98	0.16	0.82	19.8	X-ray No-flare	Poppenhaeger+ 13
N6	5763.63	0.98	0.35	0.63	18.0	X-ray No-flare	Poppenhaeger+ 13
N7	5765.88	0.99	0.54	0.46	19.8	X-ray No-flare	Poppenhaeger+ 13
N8	6600.05	0.98	0.64	0.35	35.3	X-ray No-flare	Bourrier+ 20
N9	6617.81	0.99	0.13	0.86	40.1	X-ray No-flare	Bourrier+ 20

recognized as a flare due to the very limited data points. We thus delete it from our database.

The duration of flares in Table 1 are directly taken from the original observation papers. All flares have more than three data points in their active state except for the one from Lecavelier des Etangs et al. (2012) with only one data point. So the estimate of the flare duration is reasonable by counting the time interval between the first rising and the last decaying points of the flare. For the event from Lecavelier des Etangs et al. (2012), we additionally mark the duration of this flare as <1.0 ks, which is the integration time for the only data point on the flare. On the other hand, in the selected observations each exposure time is long enough to cover the corresponding full flare event, except for the second one from Pont et al. (2007) in which only the rising part is captured. We thus mark the duration of this flare as >0.3 ks, where 0.3 ks is the length of the flare captured in the observation. For activities that occur when the planet is out of the stellar major active field region (see Figure 2), their durations are in brackets.

MRX-induced synchrotron X-ray flares usually have a larger magnitude of changes, which can be differentiated from the low-level variations in atomic lines likely due to normal changes in the stellar activity levels. So we additionally check all archive data on the X-ray observations of HD 189733 and list those without flare detection in the second half of Table 1, i.e., N1-N9. The times of these nondetections are the median time of each observation and the number in the "Duration of Burst" column is the duration of each observation. Because of the higher detectability of flares in X-ray compared to in radio bands for HD 189733 (see Route 2019), these X-ray nondetections of flares in a sense indicate the absence of significant MRX activities.

3.2. Phase Modulations of the Activities

The rotation period of HD 189733 is 11.94 ± 0.16 days and the planet's orbital period is 2.2185733 ± 0.0000019 days (Boisse et al. 2009). After transforming the activity Julian dates in Table 1 to heliocentric Julian dates, the stellar rotation and planetary orbit phases at the activity time T_0 are calculated, following Route (2019), as

$$T_0 = \text{HJD } 2453629.389 + 11.9E_{\text{rot}}, \quad (1)$$

$$T_0 = \text{HJD } 2453629.389 + 2.2186E_{\text{orb}}, \quad (2)$$

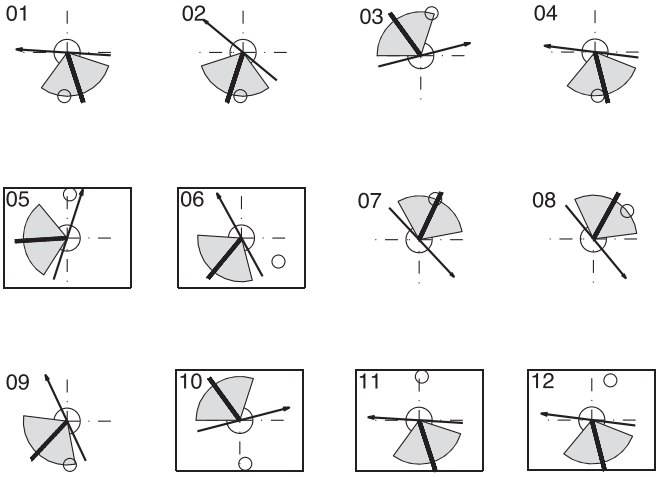

Figure 2. The major active stellar magnetic field region of HD 189733 indicated by its observed activities (with IDs in the upper left corner of each subfigure). The star is shown by the central circle, the stellar zero CML is shown by the arrow, and the planet HD 189733 b is shown by the small circle. The thick solid line is the active field line at a longitude of 112°. The gray shadow sector around the solid line is 108° in width. Seven out of the twelve activities occur when the planet is in the 108° sector, and the other five activities that occurs out of this sector are indicated by the subfigures with boxes.

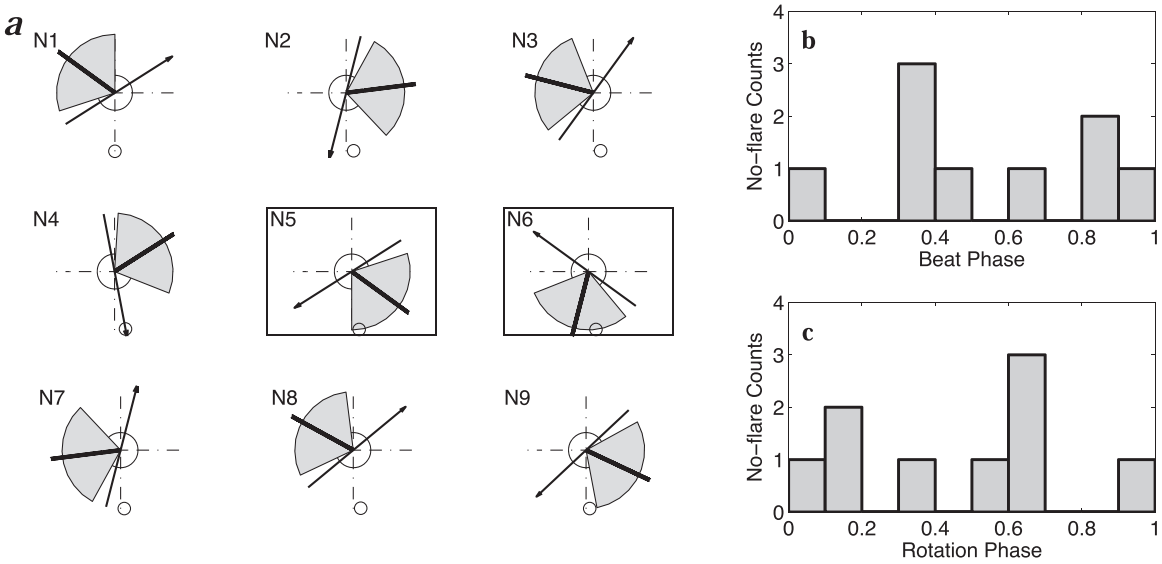

Figure 3. X-ray nondetections of flares toward HD 189733. Panel a illustrates the stellar rotation, planet orbit, and beat phases of the nondetections, with the star represented by the central circle, the stellar zero CML by the arrow, and the planet HD 189733 b by the small circle. The active field region (thick solid line with the gray shadow sector around it) is the same as in Figure 2. Panels b and c show the distributions of nondetections in the beat phase and stellar rotation phase, respectively.

where $E_{\rm rot}$ and $E_{\rm orb}$ are the stellar rotation and planetary orbit cycles, respectively, with their decimal parts representing the phases. Similarly, we define the beat cycle $E_{\rm beat}$ as

$$T_0 = \text{HJD } 2453629.389 + T_{\rm beat} E_{\rm beat}. \quad (3)$$

Considering the situation in Figure 1 that the planet orbits the star in the same direction as the stellar rotation, the beat period is $T_{\rm beat} = 2\pi/(\omega_{\rm orb} - \omega_{\rm rot}) = 2.727$ days.

The planetary orbital phases, as has been favorably selected for the transits and occultations in most of the observations, are concentrated around 0.0 and 0.5 (Table 1). The stellar rotation and beat phases do not have such a selection bias so the distributions of the activities on them represent the actual flare rate dependence. In Figures 1(b) and (c) we plot the histograms of the activity distributions, with X-ray flares shown in gray bars, to the beat and stellar rotation phases, respectively. In Figure 1(c), the distribution of the activities shows two peaks at stellar rotation phases of 0.2–0.5 and 0.7–0.9, which is consistent with previous results that X-ray flares and atomic lines are correlated with the stellar rotation (Shkolnik et al. 2008; Pillitteri et al. 2014; Fares et al. 2017). A concentration of activities between beat phases 0.6 and 0.9 is seen in Figure 1(b), which indicates the existence of a major active magnetic field region as shown in Figure 1(a). We next look into the specific location and width of this major active stellar magnetic field region.

For each of the activities listed in Table 1, we plot corresponding stellar rotation phase (with the arrows indicating the zero CML) and planetary orbit phases (with the small circle representing HD 189733 b) in Figure 2. The concentration of activities in beat phases between 0.6 and 0.9 means that these activities occur when HD 189733 b is located in a fixed sector that corotates with the star. This sector, with the solid thick line indicating the central active field line having a beat phase of 0.69 (i.e., longitude 112°) and a width of the active field region of 108° shown in gray shadow, covers 7 of the 12 activities. The activities not covered in the 108° width sector are indicated with boxes. To check whether a random distribution of activity in the beat phase can cause the current result, we can easily calculate from a binomial distribution that the possibility that 7 or more out of 12 random activities concentrate in an 108° sector, i.e., 30% of the overall beat angles, is only 2.91%. So the current distribution of activities shown in Figure 2 moderately indicates a beat phase correlation.

Such beat phase correlation is very similar to the Ganymede induced radio emission from the Jovian system (Zarka et al. 2018), and likely has an MRX origin between the exoplanet and the HD 189733 active field region. The five boxed activities in Figure 2, detected when HD 189733 b is out of this major active stellar magnetic field region, may arise from the MRX between the exoplanet and other minor stellar active field zones. The fact that these five activities with IDs 5, 6, 10, 11, and 12 have an average duration (<0.9 ks) significantly smaller than the average duration of the other seven activities (>4.1 ks) also hints at the fact that they may be induced by MRX in smaller scales; particularly, the activities 10, 11, and 12 may also be explained by the evaporation of the planetary atmosphere (Pillitteri et al. 2015; Bourrier et al. 2020). The above explanation is consistent with the knowledge of the HD 189733 magnetic field revealed from Zeeman-Doppler imaging (Fares et al. 2017), in which the stellar magnetic field is the strongest in one or two specified longitudes and has relatively weaker local peaks at other longitudes. Although the HD 189733 magnetic field structure varies due to the stellar differential rotation, Figure 6 of Fares et al. (2017) shows the existence of a major strong stellar magnetic field region at longitudes centered around ∼100°–150° for most of the time of their observations between 2007 and 2015. Our definition of the zero CML in Equation (1), shown as the arrows in Figure 2, is the same as Equation 1 of Fares et al. (2017), so the active field sector in Figure 2 with the longitude range of 58°–166° is consistent with the strong field region predicted in Fares et al. (2017).

Similar to the activities, for the X-ray nondetections of flares in Table 1 we plot their stellar rotation and planetary orbit phases in Figure 3. Different from the activities shown in Figure 2, no beat phase concentration of these observations is seen, and only two out of the nine nondetections lie in the

active field sector (N5 and N6). So there are much less interaction between the planet and the star compared to the activities shown in Figure 2.

Because MRX is a stochastic process, although it is predicted to be more frequent and violent when the planet is in the active magnetic field zone of the star, it is not necessary that one must always observe a flare at this specific beat phase. So it is not strange that we see some nondetections when the planet is in the active phase (N5, N6). On the other hand, there are detections of flares when the planet is out of the active field zone, where MRX may occur as well. There are two reasons leading to this result. First, considering the variation of the stellar active field region through 2007 and 2015 (Fares et al. 2017) during which we collected the activity observations, this major fixed active magnetic field region shown in Figure 2 may not apply for some of the activities. Second, the flares can also due to activities from the star itself, which do not correlate with the planet's orbit and the beat phase. This is similar to the Ganymede–Jupiter system, where only less than 10% of all the detected flares are correlated with the Ganymede beat period (Zarka et al. 2018).

4. Conclusion and Discussions

The concentration of HD 189733 activities in beat phase in the range of the 108° sector supports the existence of a major stellar active magnetic field region and the occurrence of SPI within it. Such SPIs are likely induced by MRX between the planet magnetic field and host stellar magnetosphere, which has a higher occurrence rate and activity level in the stellar active magnetic field region. The existence of a few activities with beat phases out of this 108° sector may arise from the existence of minor active field regions at multiple stellar longitudes; and another possible reason could be the evolution of the stellar magnetic field at timescales of months to years due to stellar differential rotation. Further observations made within a few months may rule out the variation of the stellar magnetic field. Based on the possible magnetic field interaction between a star and its close planets, it is obvious that the routine monitoring of stellar activities from a magnetically active star may help us discover its close planets through period modulation analyses.

It should be noted that because most of the current observations of HD 189733 were selected to have planetary orbital phases around 0.0 or 0.5, where a concentration of activity beat phases around 0.7 is identical to the concentration of rotation phases around 0.3 and 0.8 according to Equations (1)–(3). So the possibility that the beat phase concentration found in this paper may alternatively arise from planetary irrelevant stellar activities in fixed longitudes cannot be ruled out. Further observations with uniform selections of planet orbital phases can verify the magnetic SPI origin of flares suggested here.

The author thanks professor Tam Pak-Hin Thomas from Sun Yat-Sen University for help in analyzing the X-ray data. This work was supported by the start-up fund from Sun Yat-Sen University, and by the CAS Key Laboratory of FAST, National Astronomical Observatories.

ORCID iDs

Yang Gao https://orcid.org/0000-0002-6316-1632

References

Barnes, J. R., Haswell, C. A., Staab, D., & Anglada-Escudé, G. 2016, MNRAS, 462, 1012
Boisse, I., Moutou, C., Vidal-Madjar, A., et al. 2009, A&A, 495, 959
Bouchy, F., Udry, S., Mayor, M., et al. 2005, A&A, 444L, 15
Bourrier, V., Wheatley, P. J., Lecavelier des Etangs, A., et al. 2020, MNRAS, 493, 559
Bower, G. C., Loinard, L., Dzib, S., et al. 2016, ApJ, 830, 107
Cauley, P. W., Redfield, S., Jensen, A. G., et al. 2015, ApJ, 810, 13
Cauley, P. W., Redfield, S., & Jensen, A. G. 2017, AJ, 153, 185
Cauley, P. W., Shkolnik, E. L., Llama, J., & Lanza, A. F. 2019, NatAs, 3, 1128
Czesla, S., Klocová, T., Khalafinejad, S., Wolter, U., & Schmitt, J. H. M. M. 2015, A&A, 582, A51
Donati, J. F., Moutou, C., Malo, L., et al. 2016, Natur, 534, 662
Donati, J. F., Yu, L., Moutou, C., et al. 2017, MNRAS, 465, 3343
Fares, R., Bourrier, V., Vidotto, A. A., et al. 2017, MNRAS, 471, 1246
Fares, R., Donati, J.-F., Moutou, C., et al. 2010, MNRAS, 406, 409
Gao, Y., Qian, L., & Li, D. 2020, ApJ, 895, 22
Guilluy, G., Andretta, V., Borsa, F., et al. 2020, A&A, 639A, 49
Ip, W.-H., & Kopp, A. 2002, JGR, 107, 1491
Kaweeyanun, N., Masters, A., & Jia, X. 2020, GeoRL, 47, e86228
Lanza, A. F. 2018, A&A, 610, A81
Lecavelier des Etangs, A., Bourrier, V., Wheatley, P. J., et al. 2012, A&A, 543, L4
Lecavelier des Etangs, A., Sirothia, S. K., Gopal-Krishna, & Zarka, P. 2009, A&A, 500, L51
Maggio, A., Pillitteri, I., Scandariato, G., et al. 2015, ApJL, 811, L2
Pillitteri, I., Günther, H. M., Wolk, S. J., Kashyap, V. L., & Cohen, O. 2011, ApJL, 741, L81
Pillitteri, I., Maggio, A., Micela, G., et al. 2015, ApJ, 805, 52
Pillitteri, I., Wolk, S. J., Cohen, O., et al. 2010, ApJ, 722, 1216
Pillitteri, I., Wolk, S. J., Lopez-Santiago, J., et al. 2014, ApJ, 785, 145
Pont, F., Gilliland, R. L., Moutou, C., et al. 2007, A&A, 476, 1347
Poppenhaeger, K., Schmitt, J. H. M. M., & Wolk, S. J. 2013, ApJ, 773, 62
Route, M. 2019, ApJ, 872, 79
Shkolnik, E., Bohlender, D. A., Walker, G. A. H., & Cameron, A. C. 2008, ApJ, 676, 628
Shkolnik, E., Walker, G. A. H., & Bohlender, D. A. 2003, ApJ, 597, 1092
Shkolnik, E., Walker, G. A. H., Bohlender, D. A., Gu, P.-G., & Kürster, M. 2005, ApJ, 622, 1075
Sing, D. K., Pont, F., Aigrain, S., Charbonneau, D., & Désert, J.-M. 2011, MNRAS, 416, 1443
Smith, A. M. S., Collier Cameron, A., Greaves, J., et al. 2009, MNRAS, 395, 335
Wang, X., & Loeb, A. 2019, ApJL, 874, L23
Zarka, P. 2007, P&SS, 55, 598
Zarka, P. 2018, in Handbook of Exoplanets, ed. H. Deeg & J. Belmonte (Cham: Springer), 22
Zarka, P., Li, D., Grießmeier, J.-M., et al. 2019, RAA, 19, 23
Zarka, P., Marques, M. S., Louis, C., et al. 2018, A&A, 618, A84
Zhang, X., Ma, Q., & Artemyev, A. V. 2000, JGRA, 125, e27957